RSC Advances

PAPER

View Article Online
View Journal | View Issue

Cite this: *RSC Adv.*, 2018, **8**, 7340

4-Phenylpyrimidine monolayer protection of a copper surface from salt corrosion

N. Wei, Y. Jiang, Z. Liu, Y. Ying,* X. Guo, Y. Wu, Y. Wen and H. Yang *

Received 8th November 2017
Accepted 4th February 2018

DOI: 10.1039/c7ra12256j

rsc.li/rsc-advances

4-Phenylpyrimidine (4-PPM) containing N heteroatoms can easily form compact and uniform layers on metallic surfaces. In this work, the protection of a copper surface from corrosion in 3 wt% NaCl by a 4-PPM layer was investigated by electrochemical impedance spectroscopy (EIS) and polarization methods. Under optimum conditions, the inhibition efficiency of a 4-PPM layer for copper corrosion reached 83.2%. Raman analysis in conjunction with calculations using density functional theory (DFT) based on the B3LYP/LANL2DZ basis set suggested that the 4-PPM molecule anchored on the copper surface *via* the N_1 atom to construct a uniform layer.

1 Introduction

Copper has been used extensively in the chemical and microelectronic industries because of its outstanding electrical and thermal conductivities, corrosion resistance, and formability.[1] However, as an active metal, copper-based products still suffer from corrosion in aggressive media, especially those containing chloride ions.[2–10] Therefore, various strategies to protect copper from corrosion have been adopted, for instance, surface coating techniques. The self-assembly (SA) method as an easy layer coating assay raises particular interest since SA could lead to the formation of a dense and uniform layer on the copper surface. Organic inhibitors containing heteroatoms (in particular sulfur, phosphorous, nitrogen and oxygen) could act as coating agents and provide strong adhesive forces with metallic surfaces.

As previously reported, benzotriazole and azole derivatives are effective organic inhibitors for copper in neutral-chloride aqueous solutions.[11–13] Mercapto-organic compounds were also investigated as copper corrosion inhibitors.[14–18] Additionally, imidazole derivatives on copper surfaces were also extensively explored against corrosion.[19,20] Pyrimidine molecules containing N heteroatoms exhibited favourable protection for copper against corrosion.[21–25] In addition, 2-mercaptopyrimidine demonstrated a high efficiency for inhibiting the corrosion of copper in H_2SO_4 media.[26] 4-Phenylpyrimidine (4-PPM) molecules as shown in Scheme 1 have successfully suppressed the corrosion of cold rolled steel in HCl media.[27]

Inspired by the above successful cases, in this work, a 4-PPM solution at low concentration was prepared for self-assembling at the copper surface to form controllable, well-ordered, and compact protection layers. Using potentiodynamic polarisation and electrochemical impedance spectroscopy (EIS), the inhibition efficiency of the 4-PPM layer on the copper surface in a 3 wt% NaCl solution was evaluated. To shed light on the mechanism of molecular adsorption, further investigations by surface-enhanced Raman scattering (SERS) spectroscopy[28] and X-ray photoelectron spectroscopy were also performed.

2 Experimental

2.1 Materials and chemicals

4-PPM (97 wt% purity) was purchased from the Sigma-Aldrich Corporation. Sulfuric acid, sodium chloride and ethanol from the Sinopharm Chemical Reagents Company were of analytical grade. All solutions were prepared with Milli-Q water (18 MΩ cm).

2.2 Electrode pre-treatment

A polycrystalline copper rod (99.999% Sigma-Aldrich) in a Teflon sheath was used as a basic electrode with a geometric area of 0.0314 cm^2. Prior to the Raman and electrochemical experiments, the copper electrode was abraded using metallographic emery of 500 and 1000 grits, sequentially. 0.3 μm alumina was further used to polish the copper to obtain a shiny mirror-like surface. For the final pre-treatment, the polished

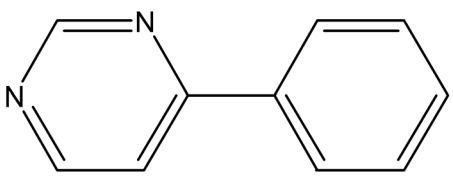

Scheme 1 Molecular structure of 4-PPM.

The Education Ministry Key Lab of Resource Chemistry, Shanghai Key Laboratory of Rare Earth Functional Materials, Department of Chemistry, Shanghai Normal University, Shanghai 200234, PR China. E-mail: hfyang@shnu.edu.cn; yingye@shnu.edu.cn; Fax: +86-02164322511

copper electrode was rinsed successively with Milli-Q water, pure ethanol and Milli-Q water to remove alumina residues and loose copper rust.

2.3 4-PPM layer modified copper electrode

The polished copper electrode was immersed into the N_2 saturated 4-PPM solution to form a 4-PPM layer assembly on the copper surface at room temperature. To obtain a dense 4-PPM coated copper surface, different 4-PPM concentrations and assembly times were carefully measured. After modification, the 4-PPM coated electrode was then taken out and rinsed thoroughly with ethanol and Milli-Q water prior to further investigation.

2.4 Electrochemical studies

The electrochemical impedance spectroscopy (EIS) analyses were carried out with a CHI750C electrochemistry workstation (CH Instruments, Inc., China) using a conventional three-electrode cell. The copper electrode without or with a 4-PPM coating was used as the working electrode, and the saturated calomel electrode (SCE) and a platinum wire served as the reference and counter electrode, respectively. All potentials were referenced against the saturated calomel electrode (*vs.* SCE). EIS results were acquired under open circuit potentials with a 5 mV (*vs.* SCE) AC amplitude and a frequency ranging from 0.01 Hz to 100 kHz. The impedance data were then interpreted based on equivalent electrical circuits (EEC) using the ZSimpWin program. The polarisation curves were measured from cathodic potential (E_{ocp} −250 mV) to anodic potential (E_{ocp} +250 mV) with a scan rate of 1 mV s^{-1}. All electrochemical measurements were carried out in a 3 wt% NaCl solution.

2.5 X-ray photoelectron spectroscopy (XPS)

The elemental composition and content of the coatings were characterised by X-ray photoelectron spectroscopy (XPS, PHI 5000 VersaProbe, Japan), with an Al Kα X-ray source (40 W, 15 KV) providing 1486.6 eV photons. The base pressure in the analysis chamber was 2×10^{-8} Pa and the test voltage was 6×10^{-7} Pa.

2.6 SERS measurements

To achieve a rough surface for SERS detection, cyclic voltammetry (CV) was carried out in a 2 M H_2SO_4 solution after the previous copper polishing pre-treatment. The potential range was set from −550 to 450 mV *versus* the saturated calomel electrode (*vs.* SCE) with a scan rate of 20 mV s^{-1} for 10 sweep segments. The final potential was held at −550 mV (*vs.* SCE) for 60 s after 5 CV cycles.

SERS measurements were taken using a confocal microprobe Raman system (LabRam II, Dilor, France). A multichannel 1024 × 800 pixel charge-coupled device was employed as a detector. A 50× long-working-length objective was used to focus a He–Ne laser line of 632.8 nm with a power of *ca.* 5 mW onto the copper surface. The confocal pinhole and slit were set at 1000 and 100 μm, respectively. Each SERS spectrum was recorded by 10 s of exposure time with 3 accumulations. Spectral calibration was done referring to the Raman line of silicon at 519 cm^{-1}.

To verify the adsorption method of 4-PPM on the copper surface, Raman spectral calculations for the 4-PPM molecule were performed using density functional theory (DFT) (B3LYP/LANL2DZ basis set) in GaussView 5. The SERS bands of the 4-PPM molecule were assigned based on the DFT computational results.

3 Results and discussion

3.1 Corrosion behaviour

EIS as a non-destructive technique could not only illustrate the impedance behaviour of the 4-PPM layer at the copper surface but could also provide information about the electrochemical kinetics at the metal/solution interface.[29] Therefore, the inhibition efficiencies of 4-PPM layers constructed at various concentrations, 0.05, 0.1, 0.5 and 1 mM, and different immersion times, 1, 3, 6 and 10 h, were characterised by EIS in a 3 wt% NaCl solution.

3.1.1 Electrochemical impedance spectroscopy. Nyquist plots along with Bode and phase angle plots of 4-PPM concentrations of 0.05, 0.1, 0.5 and 1 mM are given in Fig. 1. In Fig. 1A, the Nyquist loop of bare Cu exhibits a depressed semi-circle at high frequency and follows a straight line at low frequency. The linear portion, which inclines at an angle of 45° to the real axis, is defined as the Warburg impedance, resulting from the diffusion process of rust species[30] or the diffusion of $[CuCl_2^-; CuCl_4^{2-}]$ into the bulk solution.[31] Clearly, all the copper electrodes with 4-PPM layers formed in different concentrations show a similar trend of impedance, indicating that the formation of 4-PPM layers on the copper surface remains the same. The trend of the impedance diameter shows it first increasing then decreasing as the concentration increases, and the maximum impedance diameter is reached when the 4-PPM concentration is 0.1 mM. One possible explanation for this is that at low 4-PPM concentrations, no dense layer could be formed due to the insufficient number of 4-PPM molecules, whilst at high concentrations, 4-PPM molecules may agglomerate on the copper surface, and gradually affect the uniformity of the coating.

In the low frequency region, the $\log|Z|$ value is *ca.* 4.3 for the bare copper electrode (seen in Fig. 1B). However, for the 4-PPM modified copper, all of the $\log|Z|$ values are between 4.5 and 5.5. For 0.1 mM 4-PPM coated copper, the value reaches a maximum at 5.3, showing the most resistance against corrosion.

Additionally, in the phase angle plot, for an intact defect-free layer, the phase angle should be 90° as the resistance.[32] In the plots (see Fig. 1C) of the above-mentioned optimal concentration, *i.e.* 0.1 mM 4-PPM assembled for 6 h, the phase angle reaches a maximum (*ca.* 80°), indicating the formation of defect-less layers with promising inhibition.

Similarly, the layers formed in a 0.1 mM 4-PPM solution by adjusting the immersion time were also investigated. In Fig. 2A, the impedance diagrams are similar to each other, apart from their increased semicircle sizes, illustrating that the 4-PPM layer is getting more and more compact with the increasing assembly time. This can also be confirmed by Fig. 2B and C, where the

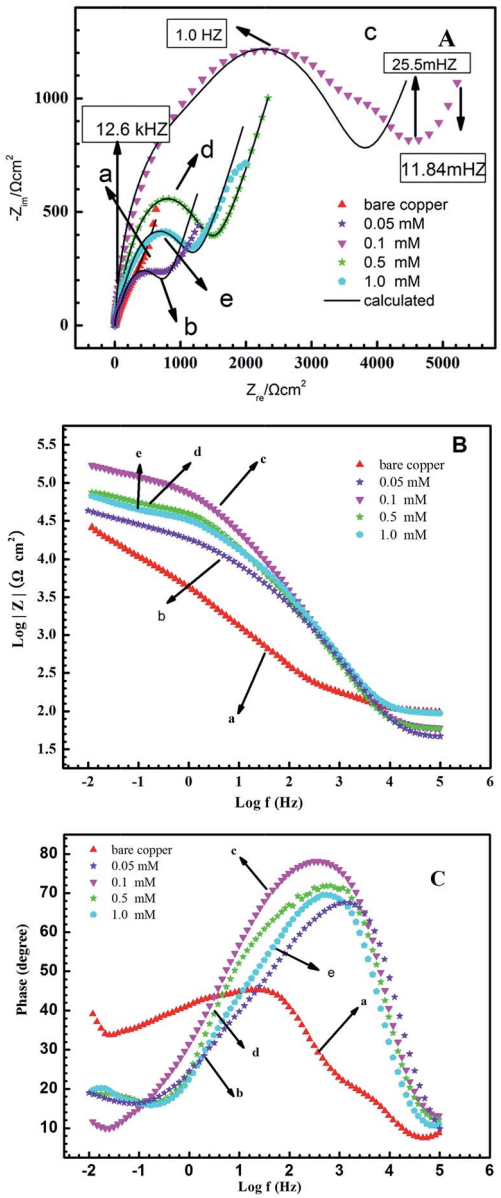

Fig. 1 (A) Nyquist, (B) Bode, and (C) phase angle plots of the copper electrodes with 4-PPM layers formed in different concentrations of 4-PPM solutions, acquired in a 3 wt% NaCl solution.

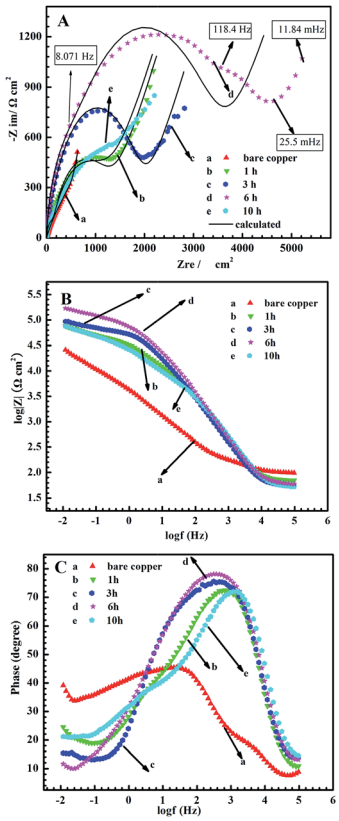

Fig. 2 (A) Nyquist, (B) Bode, and (C) phase angle plots for the copper electrodes in the absence and presence of 4-PPM layers formed in a 0.1 mM 4-PPM solution for different times, recorded in a 3 wt% NaCl solution.

Z_{mod} values and phase angles also peak when the setting time is 6 h. For the 10 h assembly time, however, a slightly different diagram shows the 4-PPM accumulation on the copper surface.

The EIS data were simulated using ZSimpWin software. The appropriate equivalent electrical circuits (EEC) in the mode of $R(Q(RW))$ for the bare copper are shown in Fig. 3a. In the case of all copper electrodes with the 4-PPM modification, $R(Q(RW))(CR)$ in Fig. 3b is more suitable. It is worth mentioning that to evaluate the accuracy of the EEC fitting models, low values of chi-squared (χ^2) (less than 10^{-3}) and least error (less than 10%) are merits.

In the equivalent circuits, R_s is the resistance of the solution, R_{ct} corresponds to the charge transfer resistance of the corrosion process at the copper/solution interface and R_f is the resistance of the 4-PPM layer at the surface with inevitable oxide species. W is the Warburg impedance due to corrosive reactant diffusion of the relevant product species. C_f represents the

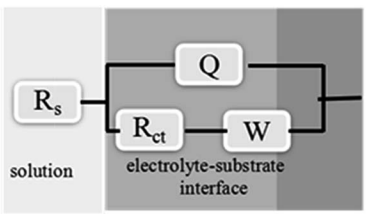

(a) R(Q(RW))

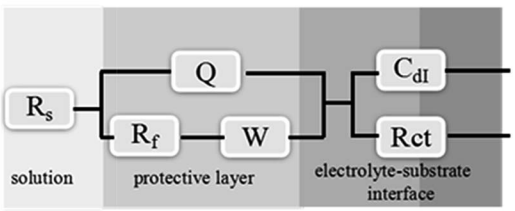

(b) R(Q(RW))(CR)

Fig. 3 Electrochemical equivalent circuits simulated for the impedance of bare copper (a), and 4-PPM modified copper (b).

Table 1 Electrochemical parameters calculated from EIS measurements for the copper electrodes with 4-PPM layers formed in different concentrations of 4-PPM solutions, in a 3 wt% NaCl solution

		Q_{dl}			W			
Concentration (mM)	R_s (Ω cm^2)	$Y_0 \times 10^{-4}$ (Ω^{-1} cm^{-2} S^n)	n	$R_{ct} \times 10^3$ (Ω cm^2)	$Y_0 \times 10^{-3}$ (Ω^{-1} cm^{-2} S$^{0.5}$)	$C_f \times 10^{-5}$ (F cm^{-2})	$R_f \times 10^2$ (Ω cm^2)	η (%)
Bare	2.95	23.6	0.567	0.571	4.48	—	—	—
0.05	1.23	1.76	0.743	0.670	4.98	2.90	0.534	21.6
0.1	1.88	0.705	0.839	2.96	2.34	3.20	4.59	83.2
0.5	1.73	0.692	0.842	1.34	2.65	4.85	0.586	59.2
1.0	2.75	0.896	0.804	1.05	3.03	2.86	0.938	49.9

Table 2 Electrochemical impedance parameters for the copper electrodes in a 3 wt% NaCl solution, in the absence and presence of layers formed in 0.1 mM 4-PPM solutions for different times

		Q_{dl}			W			
Time (h)	R_s (Ω cm^2)	$Y_0 \times 10^{-4}$ (Ω^{-1} cm^{-2} S^n)	n	$R_{ct} \times 10^3$ (Ω cm^2)	$Y_0 \times 10^{-3}$ (Ω^{-1} cm^{-2} S$^{0.5}$)	$C_f \times 10^{-5}$ (F cm^{-2})	$R_f \times 10^2$ (Ω cm^2)	η (%)
Bare	2.95	23.6	0.573	0.571	4.48	—	—	—
1	2.08	1.19	0.801	1.14	2.46	2.55	1.24	54.9
3	1.63	0.507	0.847	1.80	2.70	6.33	0.732	69.5
6	1.88	0.705	0.843	2.96	2.34	3.20	4.59	83.2
10	1.44	1.88	0.751	1.15	2.46	1.99	0.970	54.3

double layer capacitance of the 4-PPM layer, and the value for the constant phase elements (CPE) is described by the following equation:

$$Z_{CPE} = Q_{dl}{}^{-1}(j\omega)^{-n} \quad (1)$$

where Q_{dl} is the CPE constant, ω is the angular frequency, j is an imaginary number and n is the CPE exponent in relation to the degree of surface inhomogeneity, arising from surface roughness, inhibitor adsorption, and porous layer formation. In detail, when $n = 0$, Z_{CPE} is a resistance, when $n = 1$, Z_{CPE} is a capacitance, and when $n = -1$, Z_{CPE} is an inductance. Normally, the n value ranges from 0 to 1 for an electrode in a real situation. A smaller value of n corresponds to a rougher level of electrode surface morphology, hinting at serious electrode corrosion.[33]

The EIS parameters of the copper with and without 4-PPM are tabulated in Tables 1 and 2. The inhibition efficiency can be calculated by following the equation:

$$\eta\ (\%) = \frac{R_p - R_p^0}{R_p} \times 100\% \quad (2)$$

R_p^0 is the polarisation resistance of the bare copper, and R_p is the polarisation resistance of the electrode with 4-PPM. Typically, the polarisation resistance is the sum of R_{ct} and R_f.[34,35]

As shown in Tables 1 and 2, the charge transfer resistance (R_{ct}) and the layer resistance (R_f) for the copper electrode with a 4-PPM layer increase remarkably in comparison with the bare

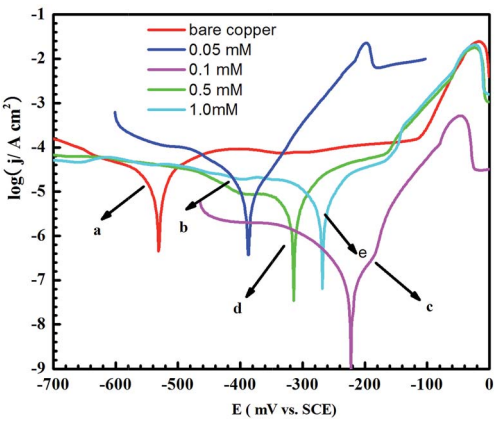

Fig. 4 Anodic and cathodic polarisation curves of the copper without and with layers formed in different concentrations of 4-PPM solutions: (a) bare, (b) 0.05, (c) 0.1, (d) 0.5, and (e) 1.0 mM, recorded in a 3 wt% NaCl solution.

Table 3 Corrosion parameters obtained from the potentiodynamic polarisation curves for copper surfaces with 4-PPM layers formed in different 4-PPM concentrations, recorded in 3 wt% NaCl solutions

Concentration (mM)	E_{corr} (V vs. SCE)	j_{corr} (μA cm^{-2})	$-\beta_c$ (V dec^{-1})	β_a (V dec^{-1})
Bare	−0.532	4.90	0.0315	0.033
0.05	−0.390	4.14	0.043	0.023
0.1	−0.233	0.018	0.037	0.032
0.5	−0.314	0.487	5.00	4.41
1.0	−0.268	0.690	1.14	7.38

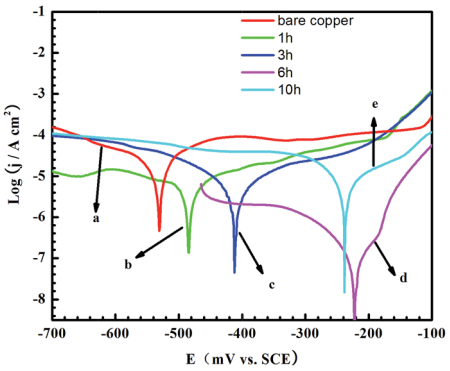

Fig. 5 Anodic and cathodic polarisation curves for copper electrodes without and with 4-PPM layers formed in 0.1 mM 4-PPM solutions for different times: (a) bare, (b) 1 h, (c) 3 h, (d) 6 h, and (e) 10 h in 3 wt% NaCl solutions.

Table 4 Polarisation parameters for the copper without and with 4-PPM layers formed in 0.1 mM 4-PPM solutions for different times, recorded in 3 wt% NaCl solutions

Time (h)	E_{corr} (V *vs.* SCE)	j_{corr} (μA cm^{-2})	$-\beta_c$ (V dec^{-1})	β_a (V dec^{-1})
Bare	−0.532	4.90	0.0315	0.033
1	−0.484	0.523	4.01	4.00
3	−0.412	0.361	6.06	4.12
6	−0.233	0.018	0.037	0.032
10	−0.238	0.537	2.25	9.70

copper, which due to the presence of 4-PPM layers sufficiently prevents the diffusion of oxygen to the copper surface. Under optimal assembly conditions of the concentration of the 4-PPM solution at 0.1 mM and an immersion time of 6 h, the peak value of R_{ct} and inhibition efficiency of copper with the 4-PPM layer are 2.96 × 10^3 Ω cm^2 and 83.2%, respectively.

3.1.2 Electrochemical polarisation studies. As shown in Fig. 4 and Table 3, in a corrosive medium of a 3 wt% NaCl solution, Tafel experimental results could be used to estimate the instantaneous corrosion rate[29] of the copper without or with an inhibitor coating, which formed in different concentrations of 4-PPM assembly solutions. Tafel curves of copper surfaces with 4-PPM layers constructed through different immersion times of electrodes in 0.1 mM 4-PPM solutions are given in Fig. 5. By extrapolating the linear anodic and cathodic branches to their intersections, the corrosion current densities (j_{corr}) and slopes (β_a and β_c) were obtained. The inhibition efficiency could also be calculated by the following equation:[36,37]

$$\eta\ (\%) = \frac{j_{corr,0} - j_{corr,i}}{j_{corr,0}} \times 100\% \quad (3)$$

where $j_{corr,0}$ and $j_{corr,i}$ are the corrosion current densities for copper electrodes without and with the 4-PPM layer, respectively. The relative parameters are summarised in Tables 3 and 4.

Compared to bare copper, it could easily be found that in the presence of 4-PPM layers, both anodic and cathodic current densities decreased, suggesting that 4-PPM mainly acted as a mixed type inhibitor at the copper surface. The j_{corr} values for all copper electrodes modified with 4-PPM are much smaller than the values for the bare copper, showing sufficient protection due to the 4-PPM layer.

3.2 Microscopic observation

The surface morphologies of copper in the absence and presence of 4-PPM layers were taken before and after immersion in 3 wt% NaCl solutions for 3 h. By comparing Fig. 6a and b, the bare copper surface after exposure to the corrosive medium exhibits some large pits. In contrast, in Fig. 6d, after 3 h immersion in a 3 wt% NaCl solution, the copper surface with a 4-PPM layer seems much smoother, showing the protection ability of the 4-PPM layer against the corrosion of copper.

3.3 XPS spectra

From the presence of C 1s and N 1s peaks in the survey spectrum, the adsorption of 4-PPM on the copper surface can be validated.

3.3.1 C 1s spectra. High-resolution XPS spectra of C 1s recorded from solid 4-PPM and copper treated with 4-PPM are shown in Fig. 7. The peak due to C 1s located at 248.8 eV (the dashed vertical line in Fig. 7a) corresponds to the C atoms in the

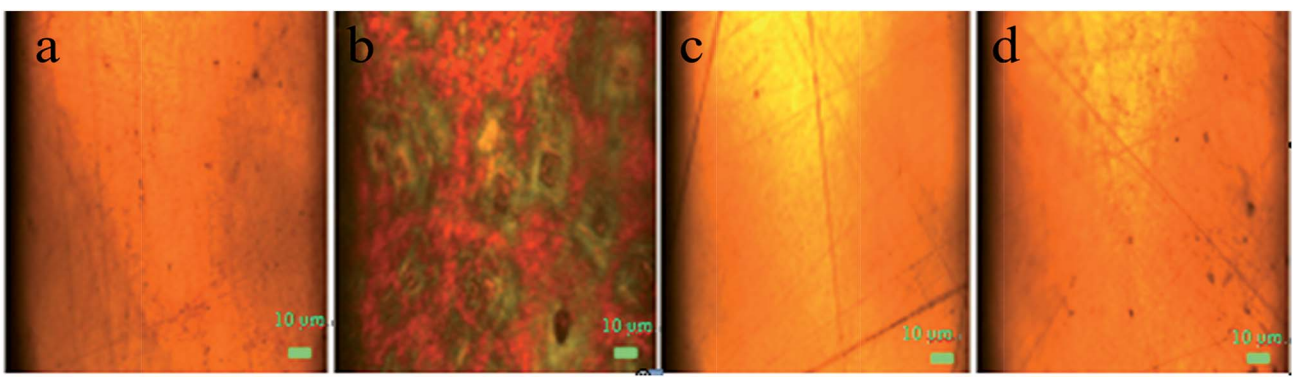

Fig. 6 Micrographs of the surfaces of (a) bare copper, (b) bare copper after immersion in a 3 wt% NaCl solution for 3 h, (c) copper with a 4-PPM layer formed in a 0.1 mM 4-PPM solution for 6 h, and (d) copper with a 4-PPM layer as shown in (c) after exposure to 3 wt% NaCl for 3 h at 298 K.

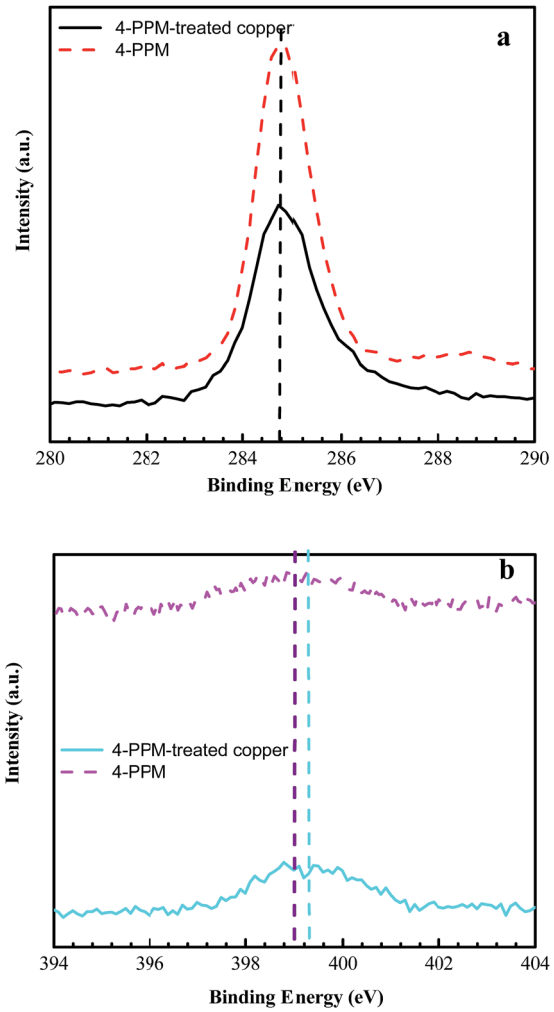

Fig. 7 (a) C 1s XPS spectra and (b) N 1s XPS spectra, recorded from solid 4-PPM and 4-PPM-treated copper.

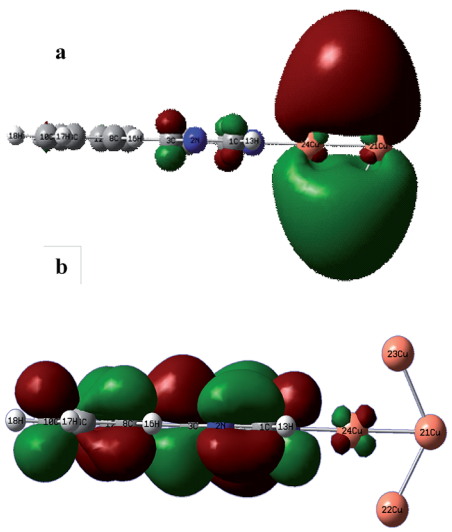

Fig. 8 Frontier molecule orbital density distributions of 4-PPM with the copper atoms.

Table 5 Quantum chemical parameters of Mulliken charges for 4-PPM

Atom	C_2	N_3	C_4	C_5	C_6	N_1
Mulliken charge	−0.287	−0.053	0.085	−0.283	−0.117	−0.280
Atom	C_7	C_8	C_9	C_{10}	C_{11}	C_{12}
Mulliken charge	0.353	−0.353	−0.222	−0.219	−0.240	−0.349

Table 6 Quantum chemical parameters for the inhibitor molecules

Molecule	E_{HOMO} (eV)	E_{LUMO} (eV)	ΔE (eV)	μ (D)
4-PPM	−0.15	−0.1	−0.05	6.52

benzene ring. The shoulder of the main peak may represent the C atom in the pyrimidine ring, which is bonded to the N atoms. On the other hand, in Fig. 7b, no significant change to the peak due to C 1s can be seen for the 4-PPM-treated-Cu, compared to bare 4-PPM. This observation suggests that the C atoms of the 4-PPM molecules might not directly bind to the copper surface.

3.3.2 N 1s spectra. N 1s spectra for the 4-PPM modified copper and the solid 4-PPM are recorded and shown in Fig. 7b. The peak due to N 1s in the 4-PPM-treated-Cu is located at about 399.2 eV while for the solid 4-PPM, the peak due to N 1s is at 399.0 eV, implying that the 4-PPM molecules might be connected to the copper surface *via* N atoms.

3.4 Quantum chemical calculations

In order to clarify the correlation between the molecular structure and its inhibition effect, quantum chemical calculations were performed. The resulting Mulliken charges of the heteroatoms and the density distribution of frontier molecular orbitals (HOMO and LUMO (see Fig. 8)) are listed in Tables 5 and 6. The larger the negative charge of an atom is, the better its adsorptive action as an electronic donor. Therefore, in Table 5, the N_1 atom with a considerably negative charge of −0.280 would anchor onto the copper surface. Further evidence is found in Fig. 8 and Table 6, where due to the HOMO being associated with the ability of a molecule to donate electrons and

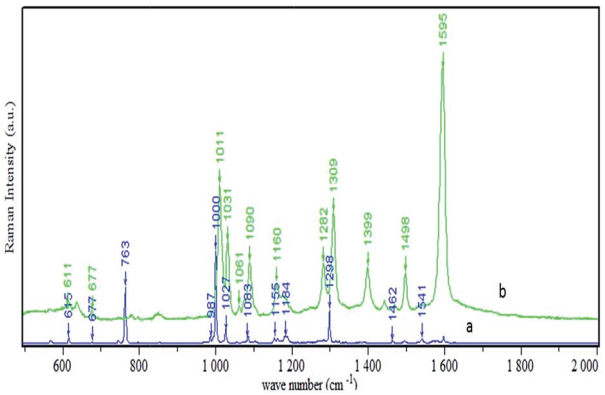

Fig. 9 (a) Normal Raman spectrum of solid 4-PPM and (b) the SERS spectrum of a 4-PPM layer on the copper electrode.

Table 7 SERS experimental results for 4-PPM and theoretical assignments according to B3LYP/LANL2DZ calculations

Solid (cm^{-1})	SERS (cm^{-1})	Calculated (cm^{-1})	Approximate assignments
615	611	633	Benzene ring rocking vibration
677	677	651	Pyrimidine ring rocking vibration; benzene ring rocking vibration
763	—	781	Pyrimidine ring stretching; benzene ring stretching
1000	—	1001	Benzene ring breathing vibration
—	1011	1016	Benzene ring stretching
1027	1031	1044	Benzene ring in-plane stretching
1083	1061	1083	Pyrimidine ring C_2–H_{13}, C_5–H_{14} in-plane rocking vibration
1155	1160	1172	Pyrimidine ring stretching
—	1282	1253	Pyrimidine ring stretching
1298	1309	1324	Pyrimidine ring C_2–H_{13}, C_5–H_{14} in-plane bending; benzene ring C_{12}–H_{20} in-plane bending
—	1393	1419	Pyrimidine ring C_2–H_{13}, C_6–H_{15} in-plane bending
1462	1498	1461	Pyrimidine ring C_2–H_{13} in-plane rocking vibration
	1595	1603	Pyrimidine ring C_5–C_6, C_2–N_1 stretching

the LUMO representing the ability of a molecule to accept electrons, it can be seen that 4-PPM can be adsorbed on the copper surface by donating the lone pair of electrons from the N_1 atom in pyrimidine to the vacant orbital of copper. The energy gap ($\Delta E = E_{LUMO} - E_{HOMO}$) is simultaneously given in Table 6 and the lower energy gap value means that the molecule is more reactive. Therefore the energy gap, ΔE of 4-PPM at −0.05 eV, indicated the trend of electron donation from 4-PPM to the copper surface. Besides, the dipole moment (μ) represents the polarity of the molecule, which is related to the inhibitive ability of a molecule. The large value of μ equalling 6.52 eV suggested that the inhibitor molecule adsorbed at the copper surface through a strong electronic force, which as a result exhibits a better inhibitive performance.

3.5 Raman studies

The normal Raman spectrum of the 4-PPM powder and the SERS spectrum for the 4-PPM layer on the copper electrode were recorded and are shown in Fig. 9. Based on the B3LYP/LANL2DZ calculations, the tentative assignments for the normal Raman and SERS bands of 4-PPM are listed in Table 7. In Fig. 9b, the strong peak at 1595 cm^{-1} is attributed to the stretching of the C_5–C_6 and C_2–N_1 bonds in the pyrimidine ring. Other intense peaks at 1309 and 1393 cm^{-1} are assignable to in-plane rocking of the C_2–H_{13}, C_5–H_{14}, C_2–H_{13}, and C_5–H_{14} bonds of the pyrimidine ring. The Raman band near 1031 cm^{-1} is due to in-

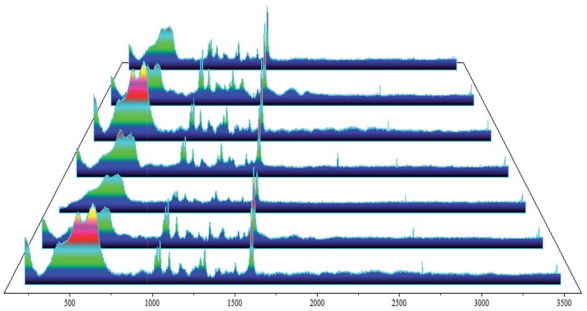

Fig. 11 SERS spectral profiles of 4-PPM layers recorded from seven randomly selected points on the copper electrode.

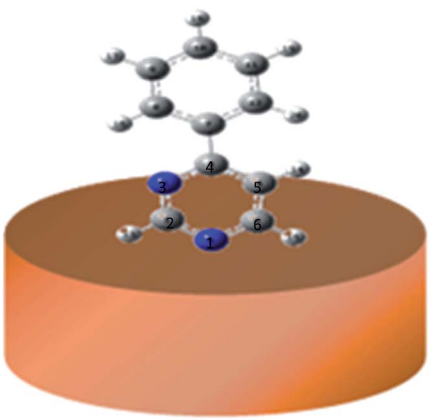

Fig. 10 Suggested adsorption model of 4-PPM molecules at the copper surface.

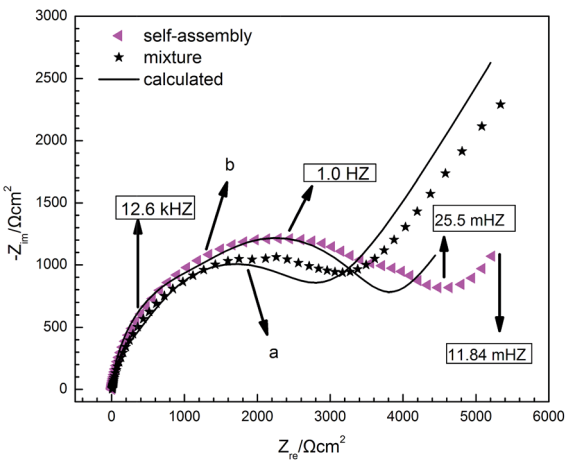

Fig. 12 Comparison of the Nyquist plots of copper electrodes with different 4-PPM layer assembly methods, acquired in a 3 wt% NaCl solution.

Table 8 Electrochemical impedance parameter comparison for different assembly methods on copper electrodes in a 3 wt% NaCl solution

		Q_{dl}			W			
Concentration (mM)	R_s (Ω cm^2)	$Y_0 \times 10^{-4}$ (Ω^{-1} cm^{-2} S^n)	n	$R_{ct} \times 10^3$ (Ω cm^2)	$Y_0 \times 10^{-3}$ (Ω^{-1} cm^{-2} S$^{0.5}$)	$C_f \times 10^{-5}$ (F cm^{-2})	$R_f \times 10^2$ (Ω cm^2)	η (%)
Bare	2.954	23.6	0.567	0.571	4.48	—	—	—
SAM	1.885	0.705	0.843	2.96	2.34	3.20	4.59	83.2
Mix	1.047	39.97	0.796	2.52	1.09	1.67	2.26	79.2

Table 9 Comparison of the inhibition efficiencies of various copper inhibitors

Inhibitor	Concentration (mM)	Medium	η (%)	References
BTAH	0.1	0.1 M KCl	70.4	Cao *et al.*[42]
DMTD	10	0.5 M HCl	84.3	Qin *et al.*[43]
T	1	0.1 M NaCl	53.5	Zucchi *et al.*[44]
MMI	1	0.5 M HCl	87.5	Larabi *et al.*[45]
4-PPM	0.1	3 wt% NaCl	79.2	This work

plane bending of the benzene ring. Additionally, the band at 1011 cm^{-1} can also be ascribed to the benzene ring stretching. The medium intensity peaks at 1081 and 1160 cm^{-1} are the contributions from in-plane rocking of C_2–H_{13} and C_5–H_{14} bonds together with pyrimidine ring stretching. According to the above analysis for the SERS bands, considering the SERS surface selection rule[38–40] in which the vibrational model where vertically attaching to or being closer to the copper surface would be enhanced, whilst conversely, the vibrational model with parallel polarisability components to the surface should not be, it could be inferred that the N_1 atom in the pyrimidine moiety of the 4-PPM molecule should be a possibly active site to adsorb on the copper surface. A schematic diagram for the adsorption fashion of a 4-PPM molecule at the copper surface is demonstrated in Fig. 10.

To illustrate the uniformity of this monolayer, SERS spectra were collected from seven randomly selected points on the copper surface coated with 4-PPM (see Fig. 11). The similar Raman peak intensities and peak positions could be used to validate the uniformity of the 4-PPM layer on the copper surface, formed by the self-assembly technique.

3.6 Corrosion comparison

In order to have a better understanding of the advantages and disadvantages of the self-assembly method used in this work compared to the conventional method,[41] an EIS comparison study was performed. For the self-assembly method, optimum assembly conditions were selected, while for the conventional method, a 3 wt% NaCl solution containing 0.1 mM 4-PPM was used as both the corrosion media and corrosion inhibitor. After the immersion of bare copper, 4-PPM will gradually adsorb on the copper surface, and will then act as a corrosion inhibitor. As shown in Fig. 12, the self-assembly method shows a bigger impedance than the conventional method does, and a better inhibition effect (the detailed parameters are shown in Table 8). Yet, for the assembly method, a considerably longer assembly time would be needed compared to the conventional method. Besides, in a real marine environment, it would be impossible to add tons of inhibitor solution into the sea water. Therefore, the self-assembly method has a bright future.

A detailed comparison of inhibition efficiency using other copper inhibitors, such as benzotriazole (BTAH),[42] 2,5-dimercapto-1,3,4-thiadiazole (DMTD),[43] tetrazole (T),[44] and 2-mercapto-1-methylimidazole (MMI),[45] is summarised in Table 9. The 4-PPM layer on the copper surface shows a considerably higher corrosion inhibition effect with lower inhibitor usage. It should be stated that for a fair comparison, for all the results in Table 9, instead of the self-assembly method used in this article, the inhibitor was mixed with corrosive media.

4 Conclusions

The use of a layer of 4-PPM on copper to prevent corrosion in a NaCl solution was investigated using electrochemical measurements. SERS techniques, XPS methods and DFT calculations were used to explore the adsorption mode of the 4-PPM molecule on the copper surface. Several conclusions could be drawn as follows:

(1) The inhibition efficiency of the 4-PPM layer formed under the optimum self-assembly conditions could reach up to 83.2%.

(2) The 4-PPM molecule adsorbed on the copper surface *via* the N_1 atom in the pyrimidine ring, and the 4-PPM molecules formed a compact, ordered and uniform layer to protect copper from salt corrosion.

(3) The self-assembly method required a considerably longer assembly time, yet resulted in a higher corrosion inhibition efficiency compared to a conventional assembly method.

Conflicts of interest

There are no conflicts to declare.

Acknowledgements

This work is supported by the National Natural Science Foundation of China (No. 21475088), the International Joint Laboratory on Resource Chemistry (IJLRC), the Science Foundation of Shanghai Normal University (No. SK201611), the Shanghai Key Laboratory of Rare Earth Functional Materials, and the

Shanghai Municipal Education Committee Key Laboratory of Molecular Imaging Probes and Sensors.

References

1 P. Wang, C. H. Liang, B. Wu, N. B. Huang and J. L. Li, Protection of copper corrosion by modification of dodecanethiol self-assembled monolayers prepared in aqueous micellar solution, *Electrochim. Acta*, 2010, **55**, 878–883.

2 A. E. Warraky, H. A. E. Shayeb and E. M. Sherif, Pitting corrosion of copper in chloride solutions, *Anti-Corros. Methods Mater.*, 1954, **51**, 52–61.

3 O. Blajiev and A. Hubin, Inhibition of copper corrosion in chloride solutions by amino-mercapto-thiadiazol and methyl-mercapto-thiadiazol: an impedance spectroscopy and a quantum-chemical investigation, *Electrochim. Acta*, 2004, **49**, 2761–2770.

4 C. W. Yan, H. C. Lin and C. N. Cao, Investigation of inhibition of 2-mercaptobenzoxazole for copper corrosion, *Electrochim. Acta*, 2000, **45**, 2815–2821.

5 K. F. Khaled, Studies of the corrosion inhibition of copper in sodium chloride solutions using chemical and electrochemical measurements, *Mater. Chem. Phys.*, 2011, **125**, 427–433.

6 M. Fonsati, F. Zucchi and G. Trabanelli, Study of corrosion inhibition of copper in 0.1 M NaCl using the EQCM technique, *Electrochim. Acta*, 1988, **44**, 311–322.

7 A. Dafali, B. Hammouti, R. Mokhlisse and S. Kertit, Substituted uracils as corrosion inhibitors for copper in 3% NaCl solution, *Corros. Sci.*, 2003, **45**, 1619–1630.

8 M. Hepel and E. Cateforis, Studies of copper corrosion inhibition using electrochemical quartz crystal nanobalance and quartz crystal immittance techniques, *Electrochim. Acta*, 2001, **46**, 3801–3815.

9 J. Mabrour, M. Akssira, M. Azzi, M. Zertoubi, N. Saib, A. Messaoudi, A. Albizane and S. Tahiri, Effect of vegetal tannin on anodic copper dissolution in chloride solutions, *Corros. Sci.*, 2004, **46**, 1833–1847.

10 L. C. Hu, S. T. Zhang, W. H. Li and B. R. Hou, Electrochemical and thermodynamic investigation of diniconazole and triadimefon as corrosion inhibitors for copper in synthetic seawater, *Corros. Sci.*, 2010, **52**, 2891–2896.

11 H. Gerengi, K. Darowicki, G. Bereket and P. Slepski, Evaluation of corrosion inhibition of brass-118 in artificial seawater by benzotriazole using Dynamic EIS, *Corros. Sci.*, 2009, **51**, 2573–2579.

12 R. M. Souto, V. Fox, M. M. Laz, M. Perez and S. Gonzalez, Some experiments regarding the corrosion inhibition of copper by benzotriazole and potassium ethyl xanthate, *J. Electroanal. Chem.*, 2000, **411**, 161–165.

13 E. Geler and D. S. Azambuja, Corrosion inhibition of copper in chloride solutions by pyrazole, *Corros. Sci.*, 2000, **42**, 631–643.

14 T. Tuken, N. Kıcır, N. TugbaElalan, G. Sıgırcık and M. Erbil, Self assembled layer based on hexane-1,6-diamine and 2-mercapto-ethanol on copper, *Appl. Surf. Sci.*, 2012, **258**, 6793–6799.

15 J. B. Matos, L. P. Pereira, S. M. L. Agostinho, O. E. Barcia, G. G. O. Cordeiro and E. D'Elia, Effect of cysteine on the anodic dissolution of copper in sulfuric acid medium, *J. Electroanal. Chem.*, 2004, **570**, 91–94.

16 H. Ashassi-Sorkhabi and E. Asghari, Effect of hydrodynamic conditions on the inhibition performance of L-methionine as a "green" inhibitor, *Electrochim. Acta*, 2008, **54**, 162–167.

17 K. Barouni, L. Bazzi, R. Salghi, M. Mihit, B. Hammouti, A. Albourine and S. E. Issami, Some amino acids as corrosion inhibitors for copper in nitric acid solution, *Mater. Lett.*, 2008, **62**, 3325–3327.

18 K. F. Khaled, Corrosion control of copper in nitric acid solutions using some amino acids-A combined experimental and theoretical study, *Corros. Sci.*, 2010, **52**, 3225–3234.

19 E. Stupnišek-Lisac, A. Gazivoda and M. Madžarac, Evaluation of non-toxic corrosion inhibitors for copper in sulphuric acid, *Electrochim.Acta*, 2002, **47**, 4189–4194.

20 R. Subramanian and V. Lakshminarayanan, Effect of adsorption of some azoles on copper passivation in alkaline medium, *Corros. Sci.*, 2002, **44**, 535–554.

21 K. F. Khaled, M. N. H. Hamed, K. M. Abdel-Azim and N. S. Abdelshafi, Inhibition of copper corrosion in 3.5% NaCl solutions by a new pyrimidine derivative: electrochemical and computer simulation techniques, *J. Solid State Electrochem.*, 2011, **15**, 663–673.

22 N. A. Al-Mobarak, K. F. Khaled, M. N. H. Hamed and K. M. Abdel-Azim, Employing electrochemical frequency modulation for studying corrosion and corrosion inhibition of copper in sodium chloride solutions, *Arabian J. Chem.*, 2011, **4**, 185–193.

23 K. F. Khaled, Studies of the corrosion inhibition of copper in sodium chloride solutions using chemical and electrochemical measurements, *Mater. Chem. Phys.*, 2011, **125**, 427–433.

24 M. E. Elshakre, H. Moustafa, H. M. E. Hassaneen and K. S. Abdullah, Electronic spectra, and DFT calculations of some triazolo[1,5-*a*] pyrimidine derivatives, *Int. J. Adv. Res.*, 2015, **3**, 703–722.

25 N. A. Al-Mobarak, K. F. Khaled, M. N. H. Hamed, K. M. Abdel-Azim and N. S. Abdelshafi, Corrosion inhibition of copper in chloride media by 2-mercapto-4-(*p*-methoxyphenyl)-6-oxo-1,6-dihydropyrimidine-5-carbonitrile: Electrochemical and theoretical study, *Arabian J. Chem.*, 2010, **3**, 233–242.

26 Z. H. Lin, F. C. Wang and Z. Q. Tian, Inhibition mechanism of 2-aminopyrimidine for copper corrosion, *Acta Phys.-Chim. Sin.*, 1992, **8**, 87–93.

27 X. H. Li, X. G. Xie, S. D. Deng and G. B. Du, Two phenylpyrimidine derivatives as new corrosion inhibitors for cold rolled steel in hydrochloric acid solution, *Corros. Sci.*, 2014, **87**, 27–39.

28 J. Chen, Y. W. Song, D. Y. Shan and E. H. Han, Modifications of the hydrotalcite film on AZ31 Mg alloy by phytic acid: the effects on morphology, composition and corrosion resistance, *Corros. Sci.*, 2013, **74**, 130–138.

29 X. Feng, S. J. Yuan, B. Liang, G. Q. Li, S. O. Pehkonen and T. J. Zhang, Superhydrophobic CuO nanoneedle-covered copper surfaces for anticorrosion, *J. Mater. Chem. A*, 2015, **3**, 4374–4388.

30 B. V. AppaRao, M. Y. Iqbal and B. Sreedhar, Self-assembled monolayer of 2-(octadecylthio) benzothiazole for corrosion protection of copper, *Corros. Sci.*, 2009, **51**, 1441–1452.

31 S. Hong, W. Chen, H. Q. Luo and N. B. Li, Inhibition effect of 4-amino-antipyrine on the corrosion of copper in 3 wt% NaCl solution, *Corros. Sci.*, 2012, **57**, 270–278.

32 Y. Y. Li, Z. Z. Yang, H. X. Qiu, Y. G. Dai, Q. B. Zheng, J. Li and J. H. Yang, Self-aligned graphene as anticorrosive barrier in waterborne polyurethane composite coatings, *J. Mater. Chem. A*, 2014, **2**, 14139–14145.

33 K. F. Khaled and N. Hackerman, Ortho-substituted anilines to inhibit copper corrosion in aerated 0.5 M hydrochloric acid, *Electrochim. Acta*, 2004, **49**, 485–495.

34 J. T. Zhang, J. Zhao, N. S. Zhang, C. T. Qu and X. Zhang, Synergized action of CuCl on recycled cigarette butts as corrosion inhibitor for N80 steel at 90° in 15% HCl, *Ind. Eng. Chem. Res.*, 2011, **50**, 7264–7272.

35 K. F. Khaled, Experimental and atomistic simulation studies of corrosion inhibition of copper by a new benzotriazole derivative in acid medium, *Electrochim. Acta*, 2009, **54**, 4345–4352.

36 R. Solmaz, Investigation of corrosion inhibition mechanism and stability of Vitamin B1 on mild steel in 0.5 M HCl solution, *Corros. Sci.*, 2014, **81**, 75–84.

37 M. Bobina, A. Kellenberger, J. P. Millet, C. Muntean and N. Vaszilcsin, Corrosion resistance of carbon steel in weak acid solutions in the presence of L-histidine as corrosion inhibitor, *Corros. Sci.*, 2013, **69**, 389–395.

38 N. Felidj, J. Aubard, G. Levi, J. R. Krenn, M. Salerno, G. Schider, B. Lamprecht, A. Leitner and F. R. Aussenegg, Controlling the optical response of regular arrays of gold particles for surface-enhanced Raman scattering, *Phys. Rev. B: Condens. Matter Mater. Phys.*, 2002, **65**, 075419.

39 A. D. McFarland, M. A. Young, J. A. Dieringer and R. P. Van Duyne, Wavelength scanned Surface-Enhanced Raman excitation spectroscopy, *J. Phys. Chem. B*, 2005, **109**, 11279–11285.

40 M. Moskovits and J. S. Suh, Surface selection rules for surface-enhanced Raman spectroscopy, calculations and application to the Surface-Enhanced Raman spectrum of phthalazine on silver, *J. Phys. Chem.*, 1984, **88**, 5526–5530.

41 N. Soltani, M. Behpour, E. E. Oguzie, *et al.*, Pyrimidine-2-thione derivatives as corrosion inhibitors for mild steel in acidic environments, *RSC Adv.*, 2015, **5**, 11145–11162.

42 P. G. Cao, J. L. Yao, J. W. Zheng, R. A. Gu and Z. Q. Tian, Comparative study of inhibition effects of benzotriazole for metals in neutral solutions as observed with Surface-Enhanced Raman spectroscopy, *Langmuir*, 2002, **18**, 100–104.

43 T. T. Qin, J. Li, H. Q. Luo, M. Li and N. B. Li, Corrosion inhibition of copper by 2,5-dimercapto-1,3,4-thiadiazole monolayer in acidic solution, *Corros. Sci.*, 2011, **53**, 1072–1078.

44 F. Zucchi, G. Trabanelli and M. Fonsati, Tetrazole derivatives as corrosion inhibitors for copper in chloride solutions, *Corros. Sci.*, 1996, **38**, 2019–2029.

45 L. Larabi, O. Benali, S. M. Mekelleche and Y. Harek, 2-Mercapto-1-methylimidazole as corrosion inhibitor for copper in hydrochloric acid, *Appl. Surf. Sci.*, 2006, **253**, 1371–1378.